VYSOKÉ UČENÍ TECHNICKÉ V BRNĚ

BRNO UNIVERSITY OF TECHNOLOGY

FAKULTA STROJNÍHO INŽENÝRSTVÍ
ÚSTAV FYZIKÁLNÍHO INŽENÝRSTVÍ

FACULTY OF MECHANICAL ENGINEERING
INSTITUTE OF PHYSICAL ENGINEERING

COULOMB INTERACTIONS IN ELECTRON BEAMS IN THE VICINITY OF A SCHOTTKY AND COLD FIELD SOURCE

COULOMBOVSKÉ INTERAKCE ELEKTRONŮ V BLÍZKOSTI SCHOTTKYHO
A STUDENÉ KATODY

ZKRÁCENÁ VERZE DIZERTAČNÍ PRÁCE
SHORT VERSION OF DOCTORAL THESIS

AUTOR PRÁCE   Ing. IVO LIŠKA
AUTHOR

VEDOUCÍ PRÁCE   prof. RNDr. BOHUMILA LENCOVÁ, CSc.
SUPERVISOR

BRNO 2010

Contents

1 Introduction

Charged particle beams are used in almost every segment of scientific research and modern industry. A wide spectrum of electron and ion beam devices is used in many specialized applications. Probably the most widely used device of this kind is an electron microscope. The history of electron microscopy began with the invention of the first device by E. Ruska and Max Knoll in 1932. In almost 80 years of research and development the number of practical applications has grown and the performance of this highly versatile tool improved dramatically. The size of studied objects is commonly few nanometers. Using high energies and special techniques also single atoms and molecules are visible. In some aspects are present-day devices working near their physical limits. Nevertheless, by optimizing the design or using new technologies and materials, the performance can be still improved.

For the electron microscopy is one of the most challenging technological segments the semiconductor industry. The development of devices utilizing charged particle optics is driven primarily by growing demands on their precision, speed, stability and reliability. Neither actual nor on-coming sub-micron manufacturing technologies would be possible without continuous innovation and performance improvements.

Recent trend towards high beam currents allows a higher throughput in electron-beam metrology and defect review. In this way the productivity can be increased and costs considerably reduced. The resolution is not the most important parameter anymore, as it practically was in the past decades. Also in other applications of charged particle beams like the material analysis by Auger electron spectroscopy (AES) and focused ion beam micro-machining (FIB) are higher beam currents necessary, although rather for technological reasons. To provide the beam with more current and conserving other important parameters, electron sources with higher brightness are required.

In systems like the scanning electron microscope (SEM) or the scanning ion microscopes is chromatic aberration the main limiting factor for the resolution. The total energy spread of the beam is hence a critical parameter for the performance of the device. The intrinsic energy spread of the emission source itself is a property of the emission surface, operational temperature and applied extraction field. Additional broadening is caused by coulomb interaction among emitted electrons that depends strongly on beam current density. Reducing the energy spread of the emission source is therefore a

2

difficult task.

The effects of coulomb interactions were studied extensively. Although some theoretical work exists, see e.g. Kruit and Jansen [1], Hawkes and Kasper [2] and a lot of experimental work and Monte Carlo simulations were published, there still remain issues where further work needs to be done. Because of high complexity of the problem, analytical approximations in source region have not been derived yet. Existing attempts are based on a large number of simplification which results into relations valid only for various special cases. A detailed Monte Carlo simulation seems to be the most suitable evaluation method presently. The coulomb interactions in currently popular liquid metal ion sources were already successfully simulated by Radlička and Lencová [3] and expected results were achieved. There is no similar detailed Monte Carlo simulation of interactions in the source region for Schottky (TFE) or cold field (CFE) emitters, which are probably the most frequently used electron sources in today's high-tech industrial and scientific electron microscopes. This work is hence focused on those emitter types. At the beginning an evaluation of the Schottky emitter only was intended.

Following chapter presents the actual state of the subject. Individual sections are devoted to brief description of standard TFE and CFE emitter, to the relevant basics of theory of electron emission from metals and to a brief overview of present analytical models for the evaluation of coulomb interactions effects. The numerical approach and available software tools are here also discussed. In Chapter 3 the main objectives of this thesis are defined. Chapter 4 presents software tools used in the simulations. The concrete emitter models and various procedures of initial data preparation and output data processing are presented. The simulation results are analyzed and discussed in Chapter 4.2.

2   The state of the art

Electron emission source is naturally a key component of every electron optical device. Generally two basic principles of electron emission are utilized in sources intended for charged particle optics. These are the thermionic and the field emission. Modern emitters are taking advantage of their combination. The selection of a suitable emitter with some specific properties depends on application requirements. For applications where low intrinsic energy width and high brightness is required, the thermal field Schottky emitter (TFE) or the cold field emitter (CFE) are the preferred choice.

2.1 Schottky and cold field emission electron source

A common Schottky emitter (fig. 1) is composed of a $\langle 100 \rangle$ oriented tungsten single-crystal wire spot welded to a heating filament. The filament is attached to two robust contact pins on a cylindrical ceramic base. The tip of the emitter (fig. 2) is electrochemically etched to a radius in the range of 0.2 - 2 μm. Bigger tip radii can be prepared using local Joule heat method [4]. At the shank of the tip is deposited a reservoir of zirconium oxide (ZrO).
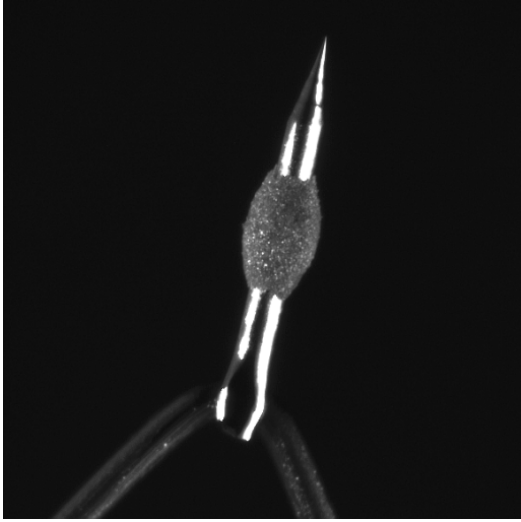

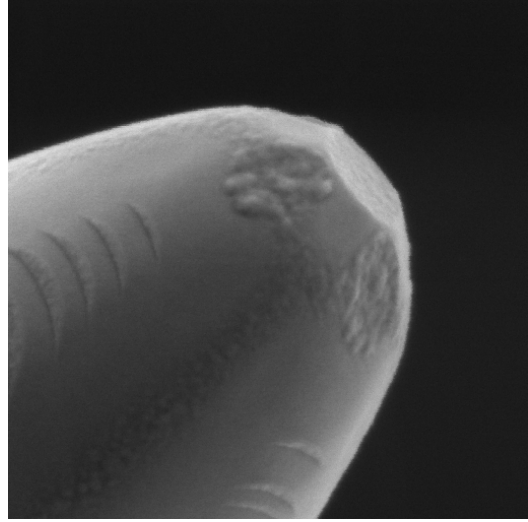Figure 1: Schottky emitter. Field of view is about 1.25 mm

Figure 2: SEM image of the emitter apex. Field of view is 1.45 μm.

Presented images of the emitter were taken by myself using light and electron microscope in the laboratory at the site of my employer, Applied Materials - ICT GmbH.

In order to achieve an electron emission from the tip, the emitter has to be heated by current in the heating filament. The typical operational temperature of the Schottky cathode is 1800K and required heating current about 2.3 A for a tip with 0.5μm radius. Strong extraction field in the range $10^7 - 10^8$ V/m combined with a relatively high operating temperature allows a material relaxation on the apex of the tip where in optimal case a stable flat facet grows after short processing. The higher temperature also ensures a continuous diffusion of zirconium oxide to the facet where an adsorbed layer lowers the work function approximately from 4.6 to 2.8eV. This effects are very important for bright and stable emission and long lifetime of the source.

Electrons emitted from the tip surface are immediately accelerated in the direction of the first positively biased electrode (extractor). The tungsten

4

wire is usually surrounded with a suppressor, which has with respect to the cathode a slightly negative voltage. The purpose of this electrode is to suppress undesired thermionic emission from the surface of the emitter behind the apex. The configuration of the electrodes used for the Schottky emitter, i.e. with a suppressor and the extractor electrode, is generally called a triode gun. Typical working point of the Schottky emitter is in the range 100 - 300 μA/sr.

The mechanical arrangement of cold field emitter is similar to the Schottky cathode, but it slightly differs in several points. The tungsten wire used for the tip has mostly $\langle 310 \rangle$ or $\langle 111 \rangle$ crystallographic orientation. Although these planes have a relatively high work function, no activation by supporting materials like oxygen or the zirconium oxide is used. The apex radius is in the range of 50 - 200 nm. A moderate electrostatic field on the extraction electrode and the small apex radius are sufficient conditions for field emission.

The CFE in principle does not need the suppressor electrode and may be operated in so called diode configuration, i.e. with the extractor electrode only. The cathode can be operated at the room temperature. The emission current is significantly less stable compared to Schottky emitter due to the very small apex radius. In order to keep the emission current as stable as possible, the required vacuum background has to be at very good level (below 1×10^{-10}Torr) and cathode needs to be frequently flashed.

Most important differences in the performance between Schottky emitter and CFE are following: CFE offers higher brightness, according to Schwind et al. [9] approximately an order of magnitude larger than Schottky emitter. Small apex area results in high emission noise. The absence of additional heating slightly lowers the energy spread to about 0.2eV. CFE has significantly higher vacuum requirements. The lifetime of Schottky cathode is under regular working conditions in average 2 years. The lifetime of the field emitter is practically unlimited until the tip is destroyed by an arc or due to improper operation. A comprehensive overview [7, 8, 5] and comparison between Schottky and CFE cathode can be found in a review paper [9].

2.2   Basic theory

The theory of emission from metal surfaces is complex. Like other rather complicated theories it introduces a number of simplifications and

assumptions. The basic one in this scope is a free-electron approximation known as the Sommerfeld model [2] derived by Sommerfeld and Bethe in 1933. It assumes among others no band structure in the bulk metal, a finite potential barrier at the surface and the Fermi-Dirac distribution for electron energies E at temperature $T > 0$. The whole emission process is influenced by many parameters and cannot be therefore described with one simple analytical expression. Most important (and freely adjustable) quantities are the temperature (T) and the field on the emitter surface (F). With respect to the T/F ratio is the spontaneous emission process divided into few categories. The thermionic emission (TE), the field emission (FE or TFE) and transitions between them (Schottky and extended Schottky emission). The principal differences among them can be better understood from the simple schematic in the Figure 3.
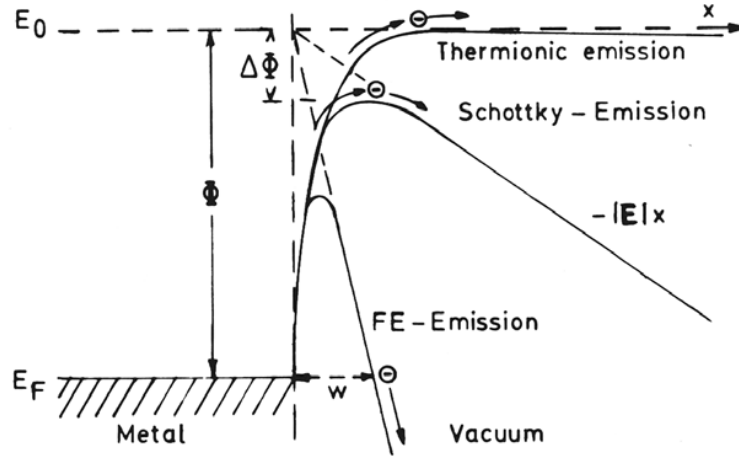
Figure 3: Emission model [11]

The hatched area on the left side are energy levels in the metal. At $T = 0$ electrons have energies only up to E_F level. On the right side is a vacuum potential E_0. In the case of *thermionic emission* (high temperature - low field) only electrons which are thermally excited according to Fermi-Dirac distribution have enough energy. They are able to overcome the potential barrier and leave the surface. The following equations are for the most part derived and in detail described in [2]. In the case of the thermionic emission can be the barrier defined by simple step function The value of the work function ϕ is a characteristic material property and represents a minimum energy needed for relocation of an electron from the material to outside. Only electrons with energy $E > \phi$ can overcome the barrier. The work function ϕ can be significantly lowered by application of some suitable surface layer (e.g.

ZrO) or also by application of electrostatic field to the cathode surface. The second possibility is known as the Schottky effect and the emission process, where the effect is involved, is called the *Schottky emission*. The potential barrier lowered by the effect of electrostatic field is defined as:

$$V(z) = \begin{cases} 0 & \text{for } z < 0, \\ \phi - eFz - e^2/16\pi\varepsilon_0 z & \text{for } z \geq 0, \end{cases} \tag{1}$$

where F is the field on the surface and z is the position on axis normal to the surface. As a reference point for the energy is taken the Fermi level E_f. If a very strong field is applied to the surface, the potential barrier is not only lower but also thinner. At the top, where the barrier is thin enough, the quantum mechanical tunneling occurs. The emission process making use of this tunneling effect is described as *Extended Schottky emission*. A precise analytical representation of the barrier is not trivial and an approximation function is used. The current density for extended Schottky mode is given by:

$$j_{ES} = j_T \, \exp\left(\frac{\Delta\phi}{kT}\right) \, \frac{\sin \pi q}{\pi q}, \tag{2}$$

where j_T is well known Richardson-Duschman equation and the parameter q can be found in [2] The $\Delta\phi$ gives the difference between the work function and the maximum of the lowered barrier:

$$\Delta\phi = \sqrt{\frac{e^3 F}{4\pi\varepsilon_0}}. \tag{3}$$

Knowing the field and appropriate current density distribution at the surface of the emitter, the starting positions of the electrons can be calculated. An important information is the total energy distribution. With the help of this function initial energies of emitted electron can be generated. By the means of the distribution function an intrinsic energy width is given. The total energy distribution of the extended Schottky emission model is given by eq.(30) in [7]:

$$dj_{ES}(E) = \frac{4\pi me}{h^3} \frac{\kappa}{1 + \exp\left(\frac{E+\phi-\Delta\phi}{kT}\right)} ln\left[1 + \exp\left(\frac{E}{\kappa}\right)\right] dE, \tag{4}$$

where the parameter κ can be found also in [2]. The appropriate angular emission distribution is also affected by strong extraction field. The

distribution function for the extended Schottky model given by eq.(44.35) in [2]:

$$R(\vartheta) = j_T \frac{(E_F - E)}{\pi d} cos(\vartheta) \cdot \exp\left[-\frac{(E_F - E)sin^2(\vartheta)}{d} \right],\qquad (5)$$

where ϑ is the polar angle and E is the energy of the particle. The last case is the *thermal-field emission*, which occurs at elevated temperature and high field on the emitter surface. Under these conditions the thermal excitation of electrons is very low and electrons are escaping from a metal only by the quantum mechanical tunneling through the field thinned barrier. The respective current density can be calculated with formula known as Murphy-Good equation:

$$j_{TF} = \frac{4\pi me}{h^3} d^2 \exp\left(b\frac{\phi}{d} \right) \frac{\sin \pi p}{\pi p},\qquad (6)$$

The last term in the eq.(6) represents a contribution of the tunneling process to the total emission. The parameter p can be again found in the [2]. The total energy distribution for the field emission model:

$$dj_{TF}(E) = \frac{4\pi me}{h^3} d \exp\left(\frac{b\phi}{d} \right) \frac{\exp(E/d)}{1 + \exp(E/d)} dE.\qquad (7)$$

The above mentioned equations are not covering all combinations of temperature, field and work function. A complete analytical theory unfortunately does not exist.

The Schottky and the field emitter are operating in virtual source mode. It means that the projected source image is not an image of the emission surface itself but of the virtual source, which is created at some position behind the apex of the emitter tip. For thermionic, Schottky and field sources are the effects of coulomb interactions neglected in absolute majority of available publications. The diameter of the virtual source is then calculated using following equation derived from geometrical and emission properties of the source [6]

$$d_{v50} = 1.67 \frac{r}{m} \sqrt{\frac{\langle E_t \rangle}{eV_{ext}}}.\qquad (8)$$

The angular magnification m is a function of emitter radius r. The parameter $\langle E_t \rangle$ is an average initial transverse energy of electrons.

Brightness is a very important beam characterizing parameter in electron optics. It help us to measure and compare the performance of electron or ion

sources. For practical purposes is generally used more convenient reduced brightness, i.e. the brightness divided by the value of the beam potential. Incorporating angular intensity and the virtual source size, the reduced brightness is given by

$$B_r = \frac{4I'}{\pi d_v^2 V_{ext}},$$ (9)

where I' is the angular current density at the extractor and d_v the virtual source size. An important property of the practical brightness is that it remains constant along the optical axis from the source down to the target, unless coulomb interaction starts to play a role.

2.3   Coulomb interactions

The effect of coulomb interactions grows with the current density in the beam. The average distance among emitted electrons is getting shorter and the influence of coulomb repulsive forces starts to play a significant role. It is most critical in the source area, in the beam crossovers and long parallel beam segments, which are created by optical components. It is also strengthened for the lower beam energies. Slower particles have more time to interact.

Coulomb interactions can affect the beam in several ways. The first and also the most pronounced way is a space charge. In the case of very high emission current density, the electrons that were not accelerated enough to escape the emitter area are creating a particle cloud in front of the tip. Their negative charge is lowering the extraction field on the emitter surface and so it acts against the emission process. This is generally typical for thermionic emitters at higher operational temperatures. Schottky and CFE emitter do not suffer from space charge in normal working mode due to their lower temperature. This effect will be therefore omitted in this work.

The second manifestation of CI is known as the Boersch effect, described in 1954. It is a statistical effect where a broadening of the particle energy distribution is caused by the stochastic coulomb interactions (after subtraction of space charge). If the chromatic aberration is dominant, it is the energy spread, which is a very important parameter. The third manifestation is the Loeffler effect (trajectory displacement effect). In this case the stochastic coulomb interactions are broadening the beam diameter and thus reducing the brightness and affecting the resolution.

Several theoretical studies were published on these subjects [12, 13, 14]. Unfortunately they do not provide any comprehensive solution. The physics of

stochastic coulomb interactions is complicated and majority of offered models are, in general, restricted to several special cases. A extensive overview of main contributors was published in [1, 14].

In published experiments and simulations are results frequently compared to two following approaches:

Knauer derived equations [12] for prediction of the energy broadening and virtual source growth in acceleration field region of the field emitter. The energy broadening is expressed as:

$$\Delta \bar{E}_z \approx 7.43 \frac{I^{2/3}}{V_0^{1/3} \alpha^{4/3} R_s^{1/3}}, \tag{10}$$

where V_0 is the beam potential, I is the beam current, R_s is an effective source radius and α is the beam half-opening angle. Basic presumption of his approximation is that steady Coulomb repulsions among particles are converting potential energy into kinetic energy. Rapidly diverging beam in the emitter area is considered as "collision free".

Jansen and Kruit [1] derived from Jansen's two-particle approximation [14] a set of analytical expressions, which are covering the Boersch and Loeffler effects for a wide range of beam geometries and operating conditions. Generally are this approximations limited to monochromatic beams with uniform current distribution propagated in the field free drift space. They do not apply to accelerating source region and the deflector areas which are treated as infinitely thin or at least the particles in the acceleration field are gaining full energy immediately after they left the emission surface or object plane. In dependence on the particle density and the beam geometry four major beam regimes are distinguished: Gaussian for very dense beams, Holtsmark for beams with moderate particle density, Lorentzian for low current densities but weak and complete collisions and a Pencil beam where the average axial distance of particles is much larger than their lateral distances. However, equations for the energy broadening and virtual spot size growth are used for this purpose also in simulations. Fransen [7] used these equations for comparison with his experimental results. He divided all terms for individual regimes by 2 in order to take only half of the crossover and the diverging part of the beam into account. The tip of the emitter is then represented by the crossover. According the Fransen the most relevant regimes are the Holtsmark and Lorentzian regime. For FW50 measure are the equations given by:

$$\Delta E_{FW50H} = 4.877 \frac{I^{2/3}}{r_c^{1/3} \alpha V^{1/3}}, \tag{11}$$

$$\Delta E_{FW50\,L} = 1.899 \cdot 10^5 \frac{I}{\alpha\, V^{3/2}}, \tag{12}$$

where the last index letter remarks particular regime, I is total current in the beam, V is beam potential. The r_c is the radius of the crossover, α is half-opening angle.

A numerical approach is frequently used in situations where stochastic effects are taking place. Coulomb interactions in charged particle beams are surely the case. The Monte Carlo is perhaps the most popular and also the most suitable numerical method for computer simulations of this kind of problems.

Several Monte Carlo simulations of coulomb interactions in the electron source region were already published among others by Shimoyama et al.(1993) [19] and Thomson (1994) [20]. They were elaborated with a diverse level of complexity. Generally a lot of approximations were introduced in the definition of initial conditions and also in the calculation method of discrete coulomb interactions. The computational performance at that time did not allow more comprehensive models.

2.4   Available software for the Monte Carlo method

Recent rapid growth of computational performance allows us to use "brute force" methods in cases where formerly a lot of limiting simplifications were required in order to reduce the calculation time. However, a simulation of coulomb effects in charged particle beams with large sets of particles is still a very demanding task. Such a complex calculations are possible only with the help of specialized software and powerful hardware. Several commercial applications are available on the market. In general, they are usually based on the finite element method (FEM), the boundary element method (BEM) or the finite difference method (FDM) which are known also from other scientific fields. The most-widely known are CPO (Charged Particle Optics) [16], Munro's Electron Beam Software (MEBS) [15], EOD (Electron Optical Design) [17] and MONTEC from Jansen's The MonTec Particle Optics Simulation Tools package [18]. Although discrete coulomb interactions can be with some of these tools calculated, they make use of various approximations that should be avoided in this work

3   The aim of the thesis

Theoretical and practical emission characteristics of the Schottky TFE and CFE cathodes were studied frequently. An extensive part of the published work is focused on the experimental evaluation of variations of the cathode operational parameters. At higher emission currents a broader energy spreads were measured than predicted in the theory. The effects of the mutual interactions among emitted particles on the energy spread and the virtual source size broadening were widely accepted as the root cause [1, 5, 4, 8]. Due to the stochastic nature of the interactions, it is impossible to measure their contribution separately. A precise Monte Carlo simulation of the emission process with the calculation of the interaction effects seems to be the most suitable tool for such a task. Several simulations focused on the coulomb interaction effects have been already performed. They are were elaborated with a diverse level of complexity, using a number of approximations.

Up to now I did not find any distinctively more detailed simulation focused on the coulomb interaction effects in the emitter region. I believe that properly defined initial conditions like the geometrically precise mesh model, the energy and the angular distribution or an extensively calculated interaction effects have a significant influence on simulation results. The aim of this thesis is to evaluate the stochastic effects of the coulomb interactions in the vicinity of the emission source using Monte Carlo simulation.

4   Methods

4.1   Software tools and procedures used in the simulation

4.1.1   The field calculation in the emitter model

In order to simulate the source region of the Schottky emitter with real-like fields, surrounding electrodes and shapes of the tip, a model based on FEM, BEM or FDM method is required. The mesh was designed using the second order finite element method (SOFEM). The main advantage of the method is the possibility of implementation of curved shapes into the mesh. It allows to model more realistic shapes of the emitter, which is usefull especially at the apex of the tip.

The potential distribution in the mesh is calculated by minimizing of energy

functional. The general form of the functional is given by:

$$U_{tot} = \frac{1}{2}\varepsilon \int \int \int \nabla \Phi \cdot \nabla \Phi \, \mathrm{d}v \qquad (13)$$

where ε is the permitivity and Φ is the potential at a general point in the mesh.
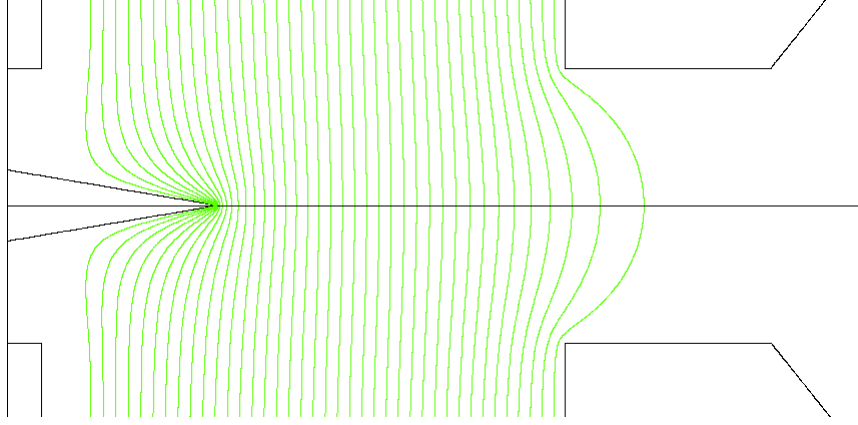

Figure 4: An example of the calculated field distribution in the emitter area. The single vertical lines represents the electrostatic field equipotentials.

The calculation of the electrostatic field within the analytical model used for the simulation of the cold field emitter model is performed in different way. A set of analytical equations is derived from the the analytical potential distribution of the model. .

4.1.2 Used programs and routines

Because the existing ray-tracing programs were not suitable for our task, a new ray-tracing routine was needed. The core of the ray-tracing program is the solver for equation of the particle motion, which is given by:

$$m\frac{\mathrm{d}^2}{\mathrm{d}t^2}\vec{r_i} = e\vec{E} + \frac{1}{4\pi\varepsilon_0}e^2 \sum_{i \neq j} \frac{\vec{r_i} - \vec{r_j}}{|\vec{r_i} - \vec{r_j}|^3}, \qquad (14)$$

where m is the mass of electron, $\vec{r}$ is the position vector, $e\vec{E}$ expresses the influence of the field and the second term on the right side of the equation is accounting for the coulomb interactions. The interactions are calculated directly, so the mutual coulomb repulsion forces between each pair of particles are evaluated.

13

The generation of initial particle data like the starting position, initial energy and starting angle is a complex procedure. It is bundled with previously presented theoretical approximations, partially emitter specific and therefore described in more detail in following sections. The requested amount of initial data needed for various simulation conditions is huge. A special program was written for this purpose.

Before the data acquired from the simulations can be analyzed, they have to be processed. It is necessary to clean the data from systematic errors, which are caused by the limitations of the simulation process. For the analysis and processing of the output data a special program has been developed.

4.2 Simulation of the Schottky emitter and the cold field emitter

4.2.1 Emitter model of Schottky TFE

Suitable emitter model is the basic condition for the simulation. A variety of cathode models were formerly proposed in published papers. Some of them were approximating the tip of the cathode by different basic shapes, that especially in the case of Schottky emitter, lead due to the absence of the flat facet to inaccurate results. For the purpose of this work a mesh model of a real Schottky emitter in triode configuration was created. Figure 5 shows full
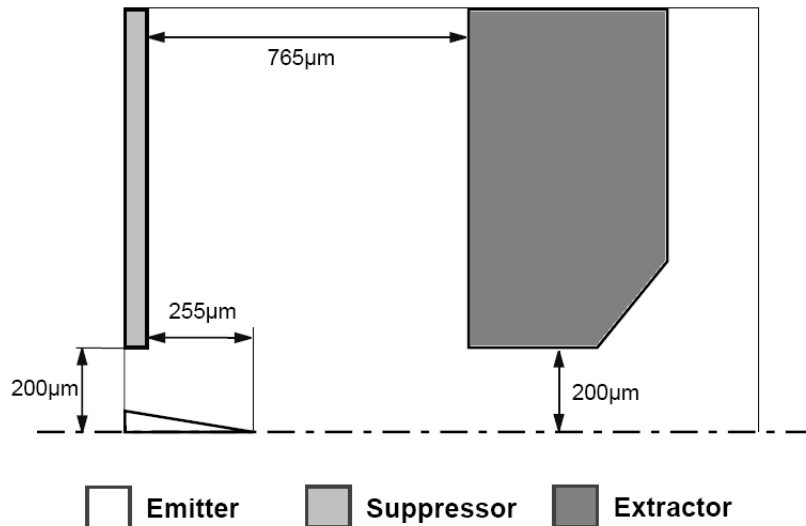

Figure 5: Sketch of the simulated Schottky emitter.

scale outline of simulated Schottky emitter with marked bore dimensions and distances between the emitter tip, the suppressor and the extractor electrode. The presented configuration is in general a standard, commercially obtainable emitter mini-module.

The simulation was performed for emitters with the tip radii 0.5, 1.0 and 1.5μm. The voltage at the suppressor is fixed on -300 V and the extractor voltage was adjusted to value on which the angular intensity of the beam reached approximately 50, 100, 200, 300 and 400 μA/sr. The area behind the extractor is considered as field free. The temperature was for all radii set to 1800K and the work function to 2.8 eV. The shape of the emitter tip was directly replicated into the mesh model from an emitter micrograph.

4.2.2 The model of field emitter

The simulation of the cold field emitter is based on an analytical model, which was initially used for a basic functionality and the precision of the ray-tracing routine. For a basic evaluation of the stochastic effects of coulomb interactions in the vicinity of the source, a simplified model is surely sufficient. A simple analytical model of pointed emitter, more precisely a diode field model, was developed by Kasper in 1978 [2]. Unlike other simple analytic approximations like a point source and a sphere model, this concept allows us to calculate a quite realistic field distribution near the tip apex and so simulate most important properties of the cathode. A detailed description of the model in a simple diode configuration can be found in [2], page 945.

The big advantage of this model are significantly lower computational demands and very smooth potential distribution in comparison with a FEM model. The value of electrostatic field $\vec{E}$ required by the equation of motion at any point of the model is given analytically. As a major drawback the model can describe the diode system only, i.e. the suppressor electrode is not included.

Three configurations with tip radius 50, 100 and 200nm were prepared. The simulations were performed for angular intensity values of 50, 100, 200, 300 and 400 μA/s.

4.2.3 Field on the surface and current density

For correct evaluation of the emission current density is the knowledge of the value of electrostatic field on the emitter surface crucial. The intensity of the field at the emitter surface depends mainly on the potential of the extractor

and the suppressor electrode, but also on several geometrical factors, like the tip radius, tip shape, the electrode spacing and bore sizes. In the case of the Schottky emitter, the presence of the flat facet on the emitter apex has a significant impact on the local field distribution. In Figure 6 is shown the calculated distribution of the electrostatic field along the emitter facet and above. The field in the middle of the rounded edge ($r = 0.025 \mu m$) is over 1.7 times higher than on the emitter axis.
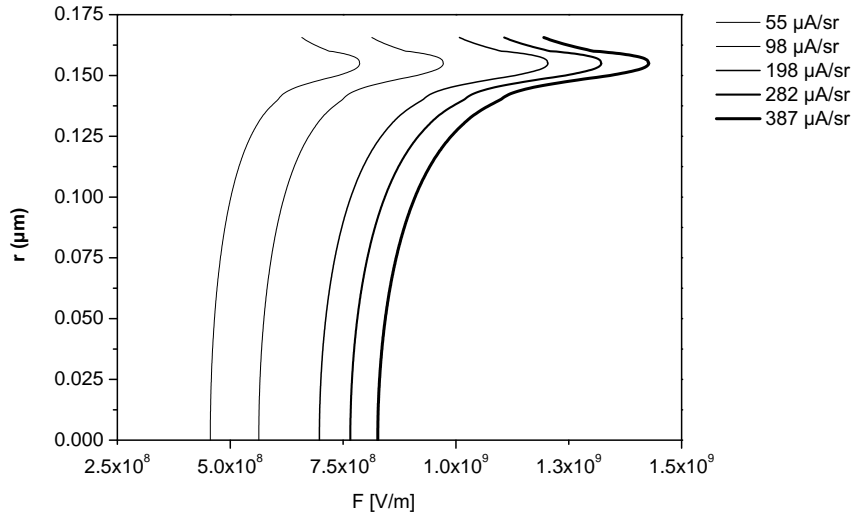

Figure 6: Surface field on emitter facet of radius $0.15 \mu m$ for several values of angular intesity.

Also in the case of the rounded tip of the cold field emitter is the strength of the field at the surface changing with the distance from the apex center, but the differences are due to the absence of the faceting small.

Knowing the field distribution at the emitter surface, the current density distribution can be calculated appropriate equations from section 2.2. If the varying electrostatic field is taken into account, in the case of the Schottky emitter, the current density value at the facet edge is about 11 times higher than on the axis, which results into factor 2 higher total emission current. The interaction effects depend strongly on the current density in the beam. From this point of view is such a difference in emission current significant and the effect of the flat facet on the electrostatic field and consequently the current density distribution has to be taken into account in the simulation. In practically all published simulations of coulomb interactions in the source area was the effect of the flat facet ignored (see section 2.3). The possible changes of the temperature and the work function along the profile of the emitter tips

16

were assumed as negligible and therefore neglected.

From the calculated current density the appropriate distribution function for the generator of random initial positions can be derived. For the purpose of the simulation of the Schottky source were used electrons emitted from the whole flat facet, the rounded edge and an additional thin stripe behind the edge in the length of 5% of the facet radius. The emission from the rounded cold field emitter tip was limited by the half angle of 16° with respect to the emitter axis.

4.2.4   Initial energy distribution

Electrons emitted from the cathode surface have some specific energy distribution. This distribution strongly depends on the emission mode, i.e. on temperature, work function and field strength. The analytical expression for the total energy distribution (TED) can be derived from the emission theory together with the equations for the current density (2) and (6), which were previously used for the generation of the particle starting positions. The energy distribution is then given by eq.(4) and (7).

For an arbitrary particle according to its location on the emission surface a field value F is determined. Subsequently the corresponding energy distribution is calculated. A random energy value from the distribution is selected and assigned to the particle. The electron-optical model of the emitter tip does not include coulomb potential. Therefore the slope of the barrier was approximated by a triangle.
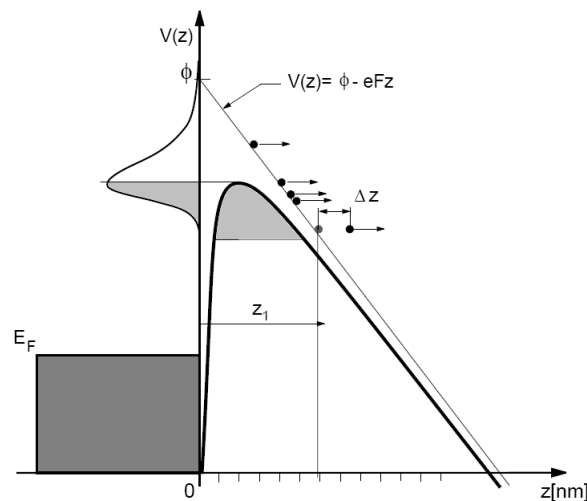

Figure 7: Barrier model

The slope of the barrier approximation is defined by:

$$V(z) = \phi - eFz \tag{15}$$

In order to model the emission process as accurately as possible, the following approach has been applied. The electrons in the metal have certain energy measured with respect to the bottom of the conduction band. If they travel towards the potential barrier (see Fig. 7), they can tunnel through and appear on the other side at the position z_1 which depends on their energy. This position would be the starting position for further simulation. Just behind the barrier the electrons would have the kinetic energy close to zero. This is problematic for the initial calculation of the electron starting angle. Therefore some small shift Δz to the initial position is introduced, which brings to the electron a corresponding shift in the energy and initial angular distribution can be calculated. The same approach is applied also for electrons with higher energy, which would normally pass above the barrier without tunneling.

4.2.5   Initial angular distribution

In the case of thermionic emission the polar angular distribution of emitted electrons is given by a simple Lambert's cosine law. If a strong field is applied to the cathode surface like in the case of the Schottky and the cold field emitter, the angular distribution is also affected. For every emitted particle a random polar angle is generated according to the Equation (5). The "shape" of the distribution is changing with the position of the electron with respect to the Fermi level and also with parameter d, which is strongly dependent on the field (see [2] page 927). The Equation (5) can be used for the whole energy range of emitted particles. Electrons at the potential barrier have the distribution influenced by the strong electrostatic field. At the top of the barrier and above is the distribution changed to simple cosine law. The azimuthal angle is randomly generated between 0 and 2π radians. In order to make the model as accurate as possible, we implemented the field-sensitive angular distribution into our emission model. In our opinion, the angular distribution has a significant effect mainly on the virtual source size of the emitter.

5   Results

5.1   The Schottky emitter

The simulation was performed for three tip radii of the Schottky TFE emitter: $0.5, 1.0$ and $1.5 \mu m$. The radius of the flat facet was 0.6 of the tip radius. The operational temperature was set to 1800K. The work function was 2.8eV. Used potential at the suppressor was -300V and the initial beam energy was set to 0V. These values were preserved in all configurations of the simulations.

5.1.1   Angular intensity and half-opening angle

The voltage at the extractor electrode was adjusted to values on which the five particular beam angular intensities should be achieved: 50, 100, 200, 300 and 400 $\mu A/sr$. A precise adjustment of the extractor voltage is not trivial. The variance of the estimated points and electron loses caused by the effect of the coulomb interactions resulted in slightly lower angular intensity values, especially at higher current densities. As already mentioned, for practical reasons, not all emitted electrons passing through the extractor hole are interesting for the analysis of the beam properties. The beam is at a distance about few millimeter after the extractor usually limited by a small aperture. The values of the angular intensity are near the optical axis sufficiently stable up to $1.5°$ for lower angular intensities and up to $2°$ for higher angular intensities. The half-opening angle limiting the beam diameter for the analysis of the simulated beam energy spread and also the size of the virtual source was within this range.

5.1.2   The energy spread

The energy spread is measured as FWHM of a curve fitted to the histogram of particle energies. The FWHM measure strongly depends on the height of the fitted maximum and is therefore very sensitive to noisy histograms. In such a cases the simultaneously calculated FW50 measure gave us more reliable results. However, the FWHM is more suitable for direct comparison with the experimental data.

The Figure 8 shows the evolution of the energy width measured as FWHM and FW50 along the z axis for several values of the angular intensity for the tip radius 0.5μm. The individual points in the graph represents measured values in a particular screen plane. A gradual growth of the energy width due to
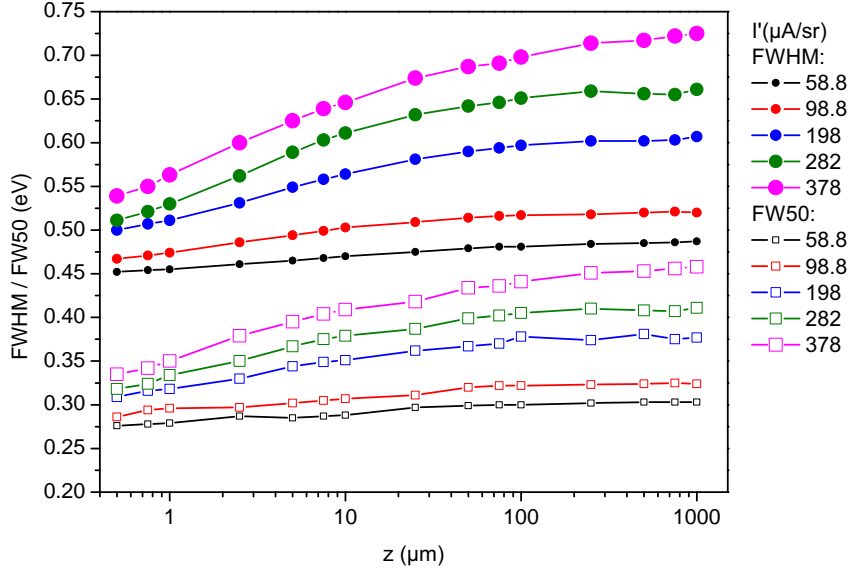
Figure 8: The evolution of the energy width for the tip with radius 0.5μm with accounting of mutual interactions

the electron-electron interactions effects is clearly visible. It is naturally more pronounced at higher emission currents, but already at the lowest simulated angular intensities is a weak energy broadening observable. Although the logarithmic scale of the horizontal axis does not display the rapid growth of the energy spread in the first 50μm so dramatically, it can be seen that the most of the broadening already took place there and further growth of the energy width is very slow. Similar procedure was repeated also for the other two tip sizes.

5.1.3 The comparison of calculated energy width with the experimental data.

Comparable experimental data for the Schottky emitter with similar parameters were published in the the paper by Sakawa et al. [4] and by Schwind et al.[9]. The used tip radii are not identical with the radii in the simulation, but they are close enough for a reasonable comparison. Other operational parameters and also the mechanical arrangement of the suppressor and the extractor are also very similar, since the evaluated emitters actually are or were based on commercially available sources, mostly produced by FEI. The experimental results as well as the simulation results have a limited accuracy, but present trends should correspond to each other in general. In this work is the comparison confined to the results published in [4] and [9].

20

Both authors evaluated electron energy spreads of emitters with several tip radii. The parameters of the emitter mechanical configuration were similar. The hard-copy of the image presenting Schwind's results was used for the comparison with performed simulations for the tip radius 0.5 and 1.0μm. Figure 9 shows the dependence of the energy spread on the reduced angular intensity.
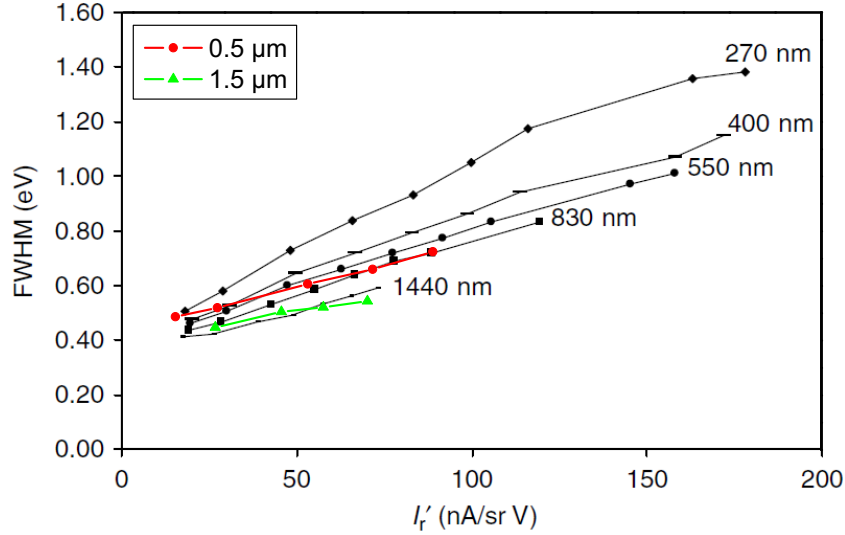

Figure 9: The comparison of calculated and measured FWHM values of the total energy distribution for tip radius 0.5 and 1.0μm. The original figure was published in [9].

The calculated data fits the measured values of the total energy spread in comparisons reasonably well. The trend lines across the simulated values have slightly different slopes. The difference between the simulation results and the experimental data at lower angular intensity is roughly 0.05eV. The presented experimental data perform at the lowest angular intensity partly better than theoretically expected. The same effect was observed also by Ohshima and Nishiyama [10]. The calculated FWHM values at high angular intensity are showing the opposite trends. They are lower than observed in experiment. The reasons for this discrepancy in this case is partly the underestimation of the current density of the analytical emission model at higher extraction field values, recently presented in [8], and probably for the most part the significantly shorter beam length in comparison with the experiment. The evolution of the calculated energy FWHM close to the screen plane shows a weak, but continuous increase. Hence, one can expect a further growth of the energy width also behind the extractor.

5.1.4 The energy broadening and comparison with analytical models

Simulations on identical initial datasets allow us to extract the exact contribution of coulomb interaction effects to the energy broadening directly from the calculated output. From both simulation runs can the actual energy E of every corresponding particle pair under desired half-opening angle be compared and the difference dE can be recorded as the contribution from the interaction effects. A histogram of recorded energies discloses the energy distribution of the broadening. The dependence of calculated and simulated FWHM energy broadening on angular intensity is shown in Figure 10.
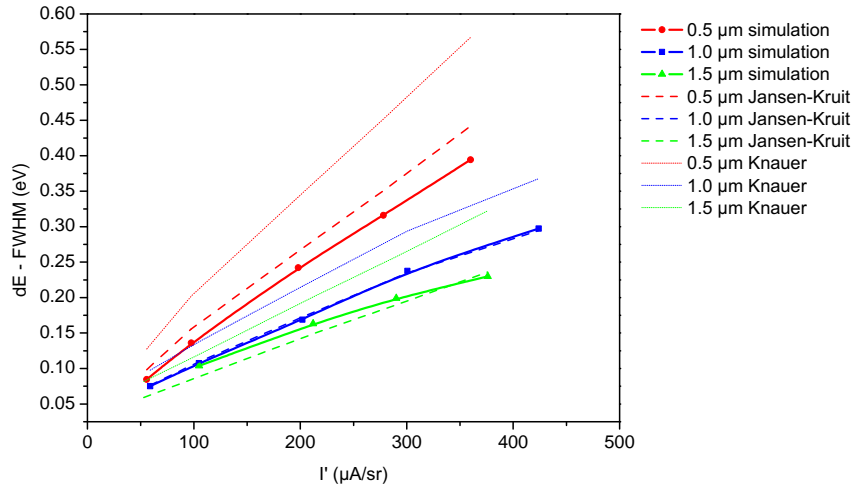

Figure 10: The comparison of the results from the simulations versus predicted values calculated from analytical approximations.

The values predicted by equation (10) proposed by Knauer are clearly overestimated. Although the equations (11)-(12) are based on a theoretical approximation, which is in general not suitable for the emitter area, the calculated curves are in a good agreement with the trend of our simulation results. The equations were derived for general beams where parameters like the total current, the beam potential, the beam half-opening angle and the size of the crossover are arbitrary, i.e. independent. In the case of a real emitter are the parameters always related to each other and consequently, they may be represented by single one in the evaluated dependence. Schwind et al. determined that the dependence of the energy broadening contribution (FW50) on I' and tip radius r obey a simple power law function. A similar function was fitted to our simulation results. The best fit was obtained for:

$$\text{FW50(Boersch)} \propto I'^{\,0.65}/r^{0.4}. \tag{16}$$

For the evaluation of the Boersch effect in the source region is such a dependence more relevant than analytical approximations presented in section 2.3. The clear linear dependence of the Boersch FW50 to the fitted function is shown in Figure 11.
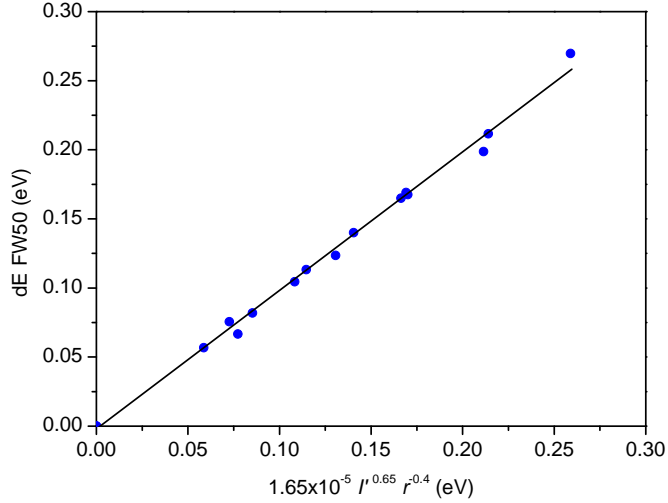

Figure 11: The Boersch FW50 versus the power function 16 shows a linear dependence.

5.1.5 The emitter brightness and the virtual source size

The reduced brightness of the source can be calculated using equation (9). The required parameters are the reduced angular intensity I'_r, i.e. the angular intensity divided by the beam potential, and the respective virtual source size d_v. All these parameters can be easily obtained from the simulation results. The calculated dependence of the virtual source size on the angular intensity is presented in Figure 12. The variations of the source size are rather small. The simulation results provide a clear trend only for the emitter with tip radius 1.0μm, where the growing angular intensity shows lowering of the virtual source size.

A direct measurements of the virtual source size are rather seldom. In various papers [9] with similar measurements of the d_v one can be found results which are closer to the analytically predicted values. It does not mean that the simulation results are wrong. The virtual source size is a source parameter, which is sensitive to the mechanical configuration and the excitation of all electron-optic components. In our case is the screen plane defined directly above the extractor electrode in the field free area. Under that conditions
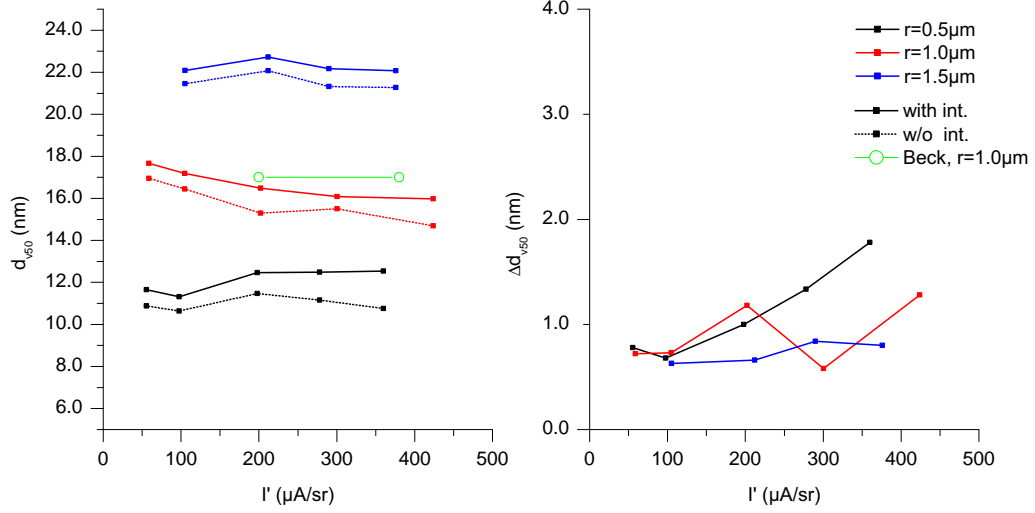
Figure 12: The resulting virtual source size and the broadening measured in the screen plane at $z = 1$mm in dependence on the angular intensity.

works the extractor as a diverging lens. The size of the virtual source is compressed. In a real electron optical device like the electron microscope or the test set-up with the energy analyzer is the beam after the extractor plane again accelerated or decelerated. Both affects the virtual source size.

The plot in Figure 13 shows that, if the brightness is the most important parameter, the relatively lower energy spread does not provide the large emitters an advantage in the performance over the smaller one. The effect of the lateral broadening on the virtual source size and herewith on brightness is due to high noise in the simulation results still in question. In general, it is small.

5.2   The CFE emitter

The simulations of the cold field emitter were performed for tip radii 50, 100 and 200nm and six angular intensity values in the range of 25 to 300μA/sr. Several screen planes were set along the z-axis behind the tip. The last screen plane was set to $z = 1$mm, i.e. to the plane of the extractor. The results are not compared to the experimental data, because of major differences in the electron-optical configuration.
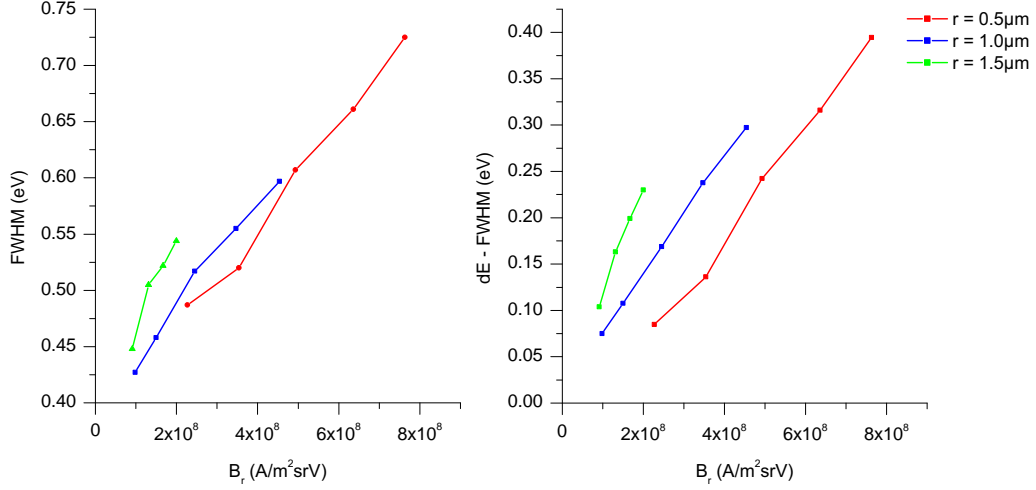
Figure 13: The energy width E and energy broadening dE measured in the screen plane at $z = 1\text{mm}$ as a function of the reduced brightness B_r.

5.2.1 The initial and total energy spread

The evolution of the energy width along the z-axis is very similar to the evolution calculated for the Schottky emitter. Also in this case the most of the energy broadening took place in the first $50\mu\text{m}$ and all simulated working points show an increase in the energy width.

In comparison with the Schottky emitter the cold field emitter is usually operated at lower angular intensity values. The reason is mainly the relatively fast increase of the energy width at higher angular intensity. In dependence on the tip radius the energy spread above $I' = 150\mu\text{A/sr}$ reach values, which are typical for the Schottky emitter. The relatively low I', usually in the range of 25–$50\mu\text{A/sr}$, does not present a problem for standard applications, because the probe current is still sufficient due to considerably higher brightness of CFE. The optimal working point is always a trade-off between the required current in the beam and the desired energy spread.

The contribution of the Boersch effect was calculated from the differences in the energy of individual particles, which were ray-traced with and without the calculation of the mutual interactions. The FWHM energy broadening dE(Boersch) versus I' is shown in left part of Figure 14. The right part of the figure shows the dependence of dE(Boersch) on the axial current density for all three tip radii.

The graphs in both parts show an outcome similar to the result from the case of the Schottky emitter. Although the emitter with 200nm tip radius has lower TED and dE values than the emitter with the smaller tip at particular
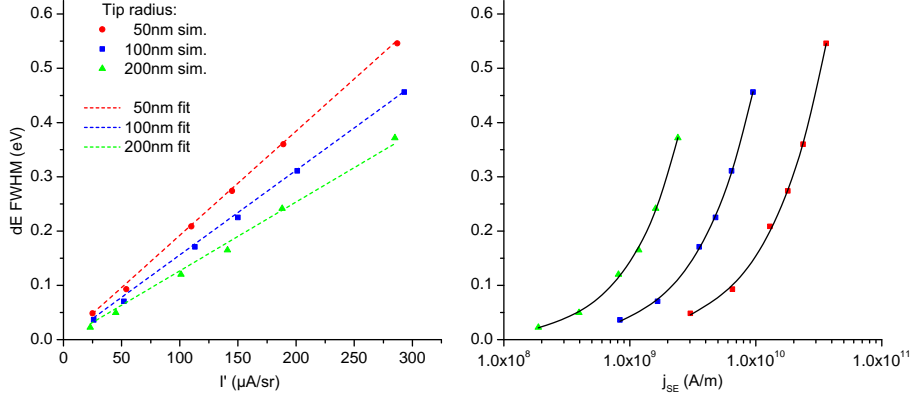
Figure 14: The dependence of dE Boersch (FWHM) on the angular intensity (left) and on the calculated axial emission current density (right).

I', the large tip suffers more from the interactions effects at the same current density level.

In the case of the cold field emitter, the values predicted by equations (11)–(12) followed distinctively different trends and a meaningful comparison was not possible. Similar to the Schottky emitter, the energy broadening contribution can be fitted to a simple power law function. The fit was successful and a linear dependence of FWHM dE(Boersch) was obtained on following function:

$$\text{FW50 dE(Boersch)} \propto I'/r^{0.3}. \tag{17}$$

5.2.2 The emitter brightness and the virtual source size

The calculation of the virtual source size d_v was performed using the same measure (FW50) and procedure like in the case of the TFE. The significantly lower tip radius r of the cold field emitter is responsible for distinctively smaller d_v in comparison with the Schottky emitter. In general, without interactions, the virtual source size decreases with the increasing extraction voltage. If the interaction effects are included, d_v is strongly affected already after few micrometers. The size of the virtual source is at $z = 1\text{mm}$ in dependence on the emitter radius and the extractor voltage up to 20 times higher. Figure 15 shows calculated d_v versus I' for all three tip radii.

The lateral broadening is more pronounced for emitters with smaller tip radius. In practice, such a small virtual source is hard to measure, apart from the fact, that d_v measured in a real optical system contains contributions of various aberrations, which have to be subtracted. In almost all related publications the virtual source size of the cold field emitter is calculated
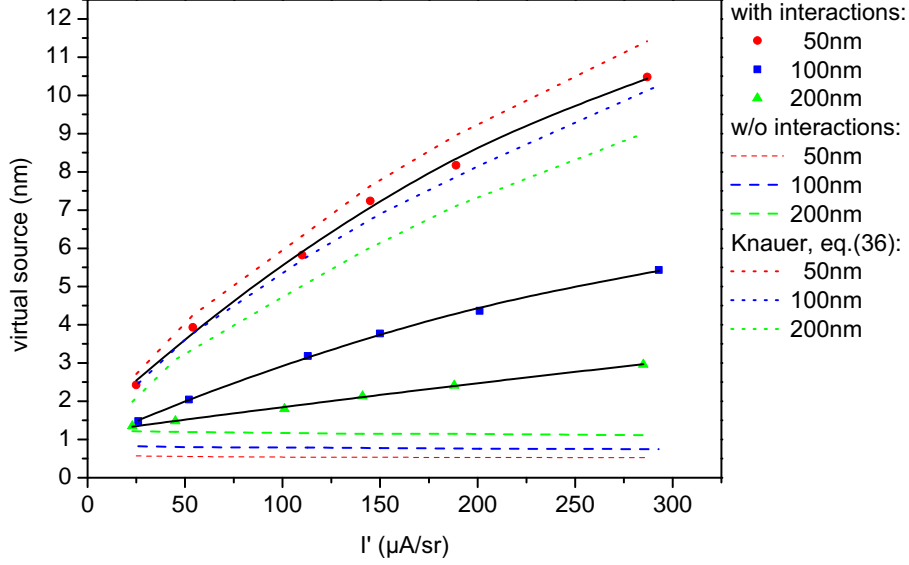
Figure 15: The calculated virtual source size d_v versus angular intensity I'. The dashed lines are values calculated without the interaction effects.

using eq. 8). The equation does not take into account the interaction effects. For our emitter model it gives values of d_v in the range of 1.7 – 3.6 nm. In comparison with relevant simulation results (i.e. d_v of the beam without calculated interaction effects) are these values approximately 3 times higher. The reason for this difference may be in a different potential distribution within the emitter area caused by the "wehnelt-like" form of the extractor electrode and the method of mirror charges.

Knowing the virtual source size, the reduced brightness B_r can be calculated using eq.(9). The B_r is indirect proportional to d_v. If d_v is by virtue of lateral interaction effects enlarged, the value of B_r is accordingly reduced. Figure 16 shows the impact of the mutual interactions on the reduced brightness.

According to our simulation results, the effect of the lateral broadening on the virtual source is relatively strong, especially for emitters with smaller tip radii. The virtual source of the smaller emitter is significantly more affected by interaction effects and the calculated brightness is accordingly lower. The emitter with 50 and 100nm tip radius show also a continuous degradation of B_r with increasing I'. The 200nm tip has a different trend at lower intensity values. At lower emission currents is the growth of I' apparently slower than the broadening of d_v and the brightness increases. This trend breaks at $I' = 100\mu\text{A/sr}$.
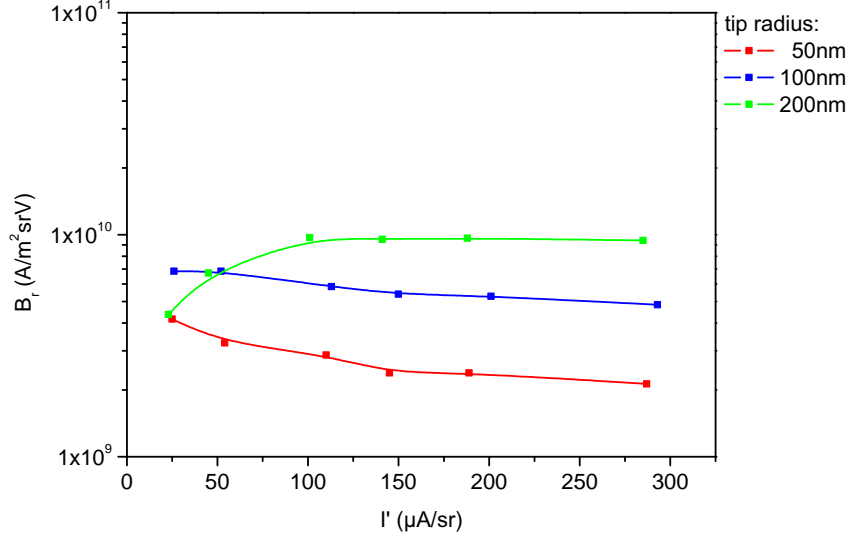
Figure 16: The calculated brightness in dependence on the angular intensity.

If the low energy spread should be preserved, the emitter should be operated at $I' \ll 150\mu\mathrm{A/sr}$ and a tip with possibly large radius should be used. Larger radius also decreases the degradation of the virtual source by the coulomb interactions. On the other hand side, it increases the intrinsic virtual source and thus some care has to be taken in order to optimize the emitter parameters to the particular need. For practical reasons, the virtual source size below approximately 5nm is difficult to work with due to the limitations caused by the aberrations of the electron lenses. Thus the increase of the virtual source size due to larger emitter radius in majority of cases does not present practical limitations.

6 Conclusion

The aim of the thesis was to prepare and perform simulation of the coulomb interaction effects in the vicinity of the field electron emitter tip using ray tracing and Monte Carlo methods. The target was to avoid simplifications or analytical approximations and thus receive results with unprecedented accuracy and reliability. Because for such a complex task no ready-to-use software exists, several specialized tools and routines have been created.

A new method for generating initial particle conditions has been developed, which respects in more detail than usually the physical emission process. A potential barrier model was introduced into the simulation of the emission process. Also the other initial data were generated using realistic models. The

28

initial angular distribution takes into account the effects of the strong surface field. The flat facet at the tip apex, typical for the Schottky emitter, was implemented. The local changes in the electrostatic field at the facet were reflected in the emission current density distribution. It has been shown that the direct effect of the facet on the initial energy width is small. However the stronger emission from the facet edge significantly contributes to the coulomb interactions.

The electron-electron interactions were calculated directly without approximation for each particle pair in the system. The simulation were very time consuming. The needed computing time for a bunch of 40000 particles was in the range of one week up to 5 months in dependence on the angular intensity and the tip radius. For every working point, i.e. the angular intensity value, were 4 bunches simulated.

The investigation concentrates on the Schottky emitter in the standard suppressor - extractor configuration. The ray-tracing of the particles was performed for three tip radii and several angular intensity values, in order to cover the typical range of operational parameters. In addition simulations were done also for cold field emitter for the set of different tip radii and angular intensities. However due to the lack of the time this simulations have been done only on the analytical field distribution model and the results can be used only for judgment of the qualitative trends not for absolute accuracy.

Some of the results were similar for both emitters: The evolution of the energy width in the emitter region showed that the absolute majority of interactions take place within first 50μm, hence the effect of interactions cannot be significantly lowered by a change of the position of the extractor. It has been shown that the magnitude of the coulomb interactions depends practically only on two parameters - on the angular intensity and on the tip radius. The dependence has a character of the power law for both parameters. The effect is proportional to the certain power of the angular intensity and inversely proportional to the power of the radius. The power coefficients depend on the particular emitter type and probably also on the geometrical parameters of the suppressor - tip - extractor configuration. However they stay within a relatively narrow range.

If not angular intensity but brightness of the emitter is parameter of the interest the character of the dependence on the emitter radius changes. For constant brightness one can get better results (less Boersch energy broadening) using emitter with smaller radius. This is because of the strong implicit dependence of the brightness on the virtual source size and thus on the emitter

radius.

The dependence of the calculated total energy width on the angular intensity was compared to available experimental data, showing a good agreement. Small differences observed in the measurements might indicate an inaccuracy of the initial energy spread predicted by the theory of the emission and effect connected with differences in the length of the beam in the experiment and in the simulation. Certain role can play also limitation of the accuracy of the experimental energy spread measurement. Schwind et al.[8] concluded a power law dependence between the Boersch effect, angular intensity and emitter radius with power coefficients similar to our results. The residual differences in the coefficients can be caused by difficult extraction of the pure Boersch energy broadening from the measured total energy distribution.

The calculated contribution of the interaction effects to the energy width was compared with predictions based on analytical approximations. It has been shown that the Knauer's formula (eq.(10)) strongly overestimates the Boersch effect and therefore is not suitable for the evaluation in similar cases. The equation (11) derived by Jansen and Kruit [1] and modified by Fransen [7] predict reasonably the tendencies, however cannot be used for quantitative estimations.

For the cold field emitter there are no reliable published data on the energy spread. According to our results the energy broadening follows similar power law as in the case of the Schottky emitter. The effect is stronger due to the smaller emitter radius and thus higher current density in the vicinity of the tip. On contrary to the Schottky emitter, the virtual source is also significantly affected by the coulomb interactions. This is due to the very small intrinsic virtual source for the typical cold field emitter. Already at moderate angular intensities the virtual source can be dominated by coulomb interactions. This is especially true for the emitter with very small radius (50nm) where the intrinsic virtual source is in the 1nm range. This can lead to the effect where the brightness reduces with increasing angular intensity due to over proportional increase of the virtual source.

References

[1] KRUIT, P. - JANSEN, G.H. Space Charge and Statistical Coulomb Effects. In *Handbook of charged particle optics*. Edited by John Orloff. New York: CRC Press LLC, 1997. 512 p. ISBN 0-8493-2513-7.

[2] HAWKES, P.W. - KASPER, E. *Principles of Electron Optics*. vol. II, New York: Academic Press, 1989. 1188 p. ISBN 0-12-333352-0.

[3] RADLIČKA, T. - LENCOVÁ, B. Coulomb interactions in Ga LMIS. *Ultramicroscopy*, 2007, vol. 108, no. 5, pp.445-454. ISSN 0304-3991.

[4] SAKAWA, S. - TSUNODA, K. - TERUI, Y. Electron emission characteristics of ZrO/W electron sources with a wide range of tip radii. *Surface and Interface Analysis*, January 2003, vol. 35, issue 1, pp.11-14. ISSN 0142-2421

[5] SWANSON, L.W. - SCHWIND, G.A. A review of the Cold-Field Electron Cathode. In. *Advances in Imaging and Electron Physics*. Academic Press, Vol.159, November 2009, pp.63-100. ISSN 1076-5670

[6] BRONSGEEST, M.S. - BARTH, G.A. - SWANSON, L.W. - KRUIT, P. Probe current, probe size and the practical brightness for probe forming systems. *J. Vac. Sci. Technol. B*, May/June 2008, vol. 26, no. 3, pp.949-955. ISSN 1071-1023

[7] FRANSEN, M.J. - FABER, J.S. - VAN ROOY, T.L. - TIEMEIER, P.C. - OVERWIJK, M.H.F - FABER, J.S. - KRUIT, P. On the Electron-Optical Properties of the ZrO/W Schottky Electron Emitter. In. *Advances in Imaging and Electron Physics*. Academic Press, Vol.111, September 1999, 372 p. ISBN 0-12-014753-X

[8] SWANSON, L.W. - SCHWIND, G.A. Review Of Zr/O Schottky Cathode. In *Handbook of charged particle optics, 2nd ed.*. Edited by John Orloff. New York: CRC Press LLC, 2009. 665 p. ISBN 978-1-4200-45543

[9] SCHWIND, G.A. - MAGERA, G. - SWANSON, L.W. Comparison of parameters for Schottky and cold field emission sources. *J. Vac. Sci. Technol. B*, Nov/Dec 2006, vol. 24, no. 6, pp.2897-2901. ISSN 1071-1023

[10] OHSHIMA, T. - NISHIYAMA, T. Study of energy distribution of Schottky emitted electrons and its theoretical analysis using effective mass

approximation. *Jpn. J. Appl. Phys.*, October 2003, vol. 42, no. 10, part 1, pp.6564-6568. DOI:10.1143/JJAP.42.6564

[11] REIMER, L. *Scanning Electron Microscopy, Physics of Image Formation and Microanalysis.* 2nd edition, Berlin: Springer, 1998. 527 p. ISBN 3-540-63976-4

[12] KNAUER, W. Energy Broadening in Field emitted Electron and Ion Beams. *Optik*, 1981, vol. 59, issue 4, pp.335-354. ISSN 0030-4026

[13] LOEFFLER, K.H. Energy Spread Generation in Electron-Optical Instruments. *Zeitschr. Angew. Phys.*, 1969, vol.27, p.257.

[14] JANSEN, G.H. Coulomb Interactions in Particle Beams. In *Advances in Electronics and Electron Physics, Suppl.21* Academic Press, 1990. 546 p. ISBN 0-12-014583-9

[15] Munro's Electron Beam Software Ltd. [online]. last modified 13 February 2008. [cit. 2004-04-20]. URL:<http://www.mebs.co.uk/>

[16] CPO Ltd.: Help for CPO Programs. CPO Ltd, UK, Feb 2001, Version 3.1e. URL:<http://www.electronoptics.com/>.

[17] LENCOVÁ, B. - ZLÁMAL, J. The Development of EOD Program for the Design of Electron-Optical Devices. *Microscopy and Microanalysis*, 2007, vol. 13, suppl. 3, pp. 2-3. ISSS 1431-9276

[18] Caneval BV - Montec.: Manual for MONTEC and INTERAC. Caneval BV, Netherlands, Jan 2004, Version 1.7.
URL:<http://www.caneval.com/montec/downloads/MonTec_Manuals.pdf>.

[19] SHIMOYAMA, H. - SHIMAZAKI, Y. - TANAKA, A. Computer simulation of energetic Boersch effect in the diode region of the field emission gun. In *SPIE - Charged Particle Optics*, September 1993, vol. 2014, pp.99-103. ISBN 0-8194-1263-5

[20] THOMSON, M.G.R. Electron-electron scattering in microcolumns. *J. Vac. Sci. Technol. B*, Nov/Dec 1994, vol. 12, no. 6, pp.3498-3502. ISSN 0734-211X

32

Ing. Ivo Liška
Curriculum Vitae

Osobní údaje

Datum narození:	6. července 1976
Kontaktní adresa v ČR:	Hraniční 260
	747 24 Chuchelná
Kontaktní adresa v SRN:	Jagdfeldring 25
	85540 Haar
	Německo
Kontaktní telefon:	+49 89 909994 51
e–mail:	ivo_liska@amat.com
Rodiný stav:	ženatý, 2 děti

Pracovní činnost

Applied Materials, ICT GmbH Německo 2002 – dosud

Zaměstnán jako fyzik ve vývojovém oddělení elektronové mikroskopie

Dosažené vzdělání

Postgraduální studium - kombinovaná forma 2002 – dosud

Fakulta strojního inženýrství, Vysoké učení technické v Brně
Obor: Fyzikální a materiálové inženýrství, školitel prof. doc. RNDr. Bohumila Lencová, CSc., ÚPT AV ČR, Brno.
Téma dizertační práce: Coulombovské interakce elektronů v blízkosti Schottkyho a studené katody

Vysokoškolské vzdělání 1997 – 2002

Fakulta strojního inženýrství, Vysoké učení technické v Brně, obor: Fyzikální inženýrství
Téma diplomové práce: Určování struktury povrchu pevných látek metodou LEED.
Školitel: Doc. Tomáš Šikola, CSc., vedoucí diplomové práce: Ing. Jaroslav Jiruše.

Středoškolské vzdělání 1990 – 1994

Vojenské gymnázium Opava.

Další zkušenosti

2001 – čtyřměsíční stáž (projekt ERASMUS) na Aston University, Birmingham (UK).

Jazykové znalosti

Aktivní znalost anglického a německého jazyka slovem i písmem.
Pasívní znalost ruského a polského jazyka.

Abstract

This thesis deals with the effects of the coulomb interactions in the vicinity of the Schottky and the cold field electron source. It provides a basic overview about the subject describes Monte Carlo simulation method and used emitter models. A new method for generating initial particle conditions has been developed, which respects in more detail than usually the physical emission process. Especially the effects of the mutual interactions on energy width, size of the virtual source and brightness in dependence on the tip radius and the angular intensity were investigated. The evolution of the energy width in the emitter region showed that the absolute majority of interactions take place within first few micrometer. The dependence of the calculated total energy width on the angular intensity was compared with available experimental data, showing a good agreement. The calculated contribution of the interaction effects to the energy width was compared with predictions based on analytical approximations. It has been shown that some of them predict reasonably the tendencies but cannot be used for quantitative estimations.